Hindawi
Wireless Communications and Mobile Computing
Volume 2022, Article ID 4987990, 19 pages
https://doi.org/10.1155/2022/4987990

Research Article

Sparse Covariance Matrix Reconstruction-Based Nulling Broadening for UAV 2D Antenna Arrays

Chuang Han, Haoyang Lei, Yanyun Gong, and Ling Wang

The School of Electronics and Information, Northwestern Polytechnical University, Xi'an, Shaanxi 710072, China

Correspondence should be addressed to Ling Wang; lingwang@nwpu.edu.cn

Received 2 December 2021; Revised 22 January 2022; Accepted 23 March 2022; Published 10 May 2022

Academic Editor: Bo Rong

Since the antennas on UAVs may have slight vibrations or the interference source is in the state of rapid movement in practice, the interference suppression performance and robustness of the traditional methods may suffer a decline. In this paper, we propose a flexible asymmetric null widening technique, which allows flexible adjustment of the null width to accommodate the variation of the interference source. This method has a good effect of spreading zero trap on the two-dimensional array and can effectively reduce the waste of degrees of freedom. Firstly, the flexible asymmetric null widening method is extended to two-dimensional arrays to accommodate 2D array antennas of UAVs. Secondly, when the SMI algorithm is applied in adaptive beamforming, the desired signal appears in sampling snapshots or using data samples, resulting in a model mismatch. To solve the model mismatch problem of UAV antenna arrays, this paper applies a sparsity-based interference plus noise covariance matrix reconstruction technique. Finally, for the application scenario that the UAV may receive signals from multiple directions, we apply the linear constrained minimum variance criterion (LCMV) to achieve the main beam gain formation in multiple directions. The simulation results show that we can generate a wide null and adjust the null width asymmetrically. The results also show that the model mismatch problem is avoided, and the performance of the adaptive beamforming is almost optimal. For the UAV antenna, we also implemented multiple beams to receive multiple signals .

1. Introduction

In recent years, drones have been widely used in various fields, including aerial photography, target detection, crop condition monitoring, and marine remote sensing [1–4], while in the communication between UAVs or UAVs in receiving the desired target signal, the UAV's receiving antenna needs to process the received signal, i.e., array signal processing, and its core is adaptive array processing also known as airspace adaptive filtering. It is now widely used in military and civilian applications in radar, sonar, seismology, radio astronomy, wireless communications, acoustics, medical imaging, and other fields [5–9]. It is well known that adaptive beamforming techniques are sensitive to model mismatch, especially when the desired signal is present in the training data. In addition, as the absolute stability of UAVs cannot be guaranteed during flight, the antenna may have slight vibration or the unstable interference signal source may have fast movement, resulting in interference signal deviation. As a result, the adaptive beamforming cannot suppress the deviated interference signal effectively. For these reasons, the performance of traditional adaptive beamformers deteriorates severely. Therefore, robust adaptive beamforming methods have been extensively studied in the past decades, and many robust adaptive beamforming methods have been proposed. In adaptive beamforming, the classic method of minimum variance distortion response (MVDR) [5, 10], also known as Capon beamforming [11], is generally adopted to obtain the weight of beamforming. However, since the ideal sampling covariance matrix cannot be obtained, the sampling covariance matrix inverse algorithm (SMI) [12] is used in practice. Because the SMI algorithm uses sampling data to construct the covariance matrix, it is possible to include information about the desired signal in the covariance matrix. This means that the results are influenced by the expected signal. In the case that the signal-to-noise ratio (SNR) is high, the results can be significantly mismatched, leading to a severe decline in

beamformer performance. Typically, diagonal loading techniques [13] are used to solve these problems, but due to the difficulty of finding the optimum diagonal loading factor for the corresponding beamformer. Worst-case performance optimization [14], on the other hand, can also be considered as a diagonal loading technique. However, the worst-case scenario does not always occur, and the optimization results are still suboptimal. An adaptive tridiagonal loading technique has also been proposed [15], where the unitary matrix is replaced by a Toplitz matrix and the loading factor is determined by a method based on the output power of a low partials beam in the assumed direction of the desired signal. However, since the information of the desired signal is still retained, the performance is improved over other beamformers at large signal-to-noise ratios but still decreases as the signal-to-noise ratio increases. Another solution to the mismatch problem is to deal with the assumed signal guidance vector. Since the mismatch vector and its parametric bound are actually unknown, the actual guidance vector can be estimated in an iterative manner, with each iteration being a quadratic convex optimization problem [16]. In this paper, in order to solve the mismatch problem in UAV antenna beamforming, a better approach is to reconstruct the covariance matrix to remove the information of the desired signal and then directly solve the mismatch problem caused by the desired signal [17]. To reduce the computational effort associated with covariance matrix reconstruction, the sparse nature of the signal source in the observed field in UAV antenna beamforming is used to reconstruct the covariance matrix [18].

Since the UAV cannot be absolutely stable in the flight process and the location of interference sources in the environment cannot be absolutely unchanged, the interference signals to be suppressed by the UAV antenna will deviate slightly. In traditional adaptive beamforming, only a single interference signal cannot produce a zero trap, so it is necessary to broaden the width of the zero trap at the interference. To solve the above problems, the classic zero-trap broadening method is the covariance matrix conization technique (CMT) [19]. It is mainly realized by using a null widening technology independently proposed by Zatman [20] and Mailloux [21], which can obtain a wider zero trap. Much further work has been done based on covariance matrix conization (CMT). A novel null widening method for sidelobe cancellers with high computational efficiency is proposed [22]. The CMT technique can produce a wide zero trap, and it produces the widest zero trap to cover the worst case of interfering signal deviation, which causes it to waste a large number of degrees of freedom [23]. It shows that the cost of degrees of freedom is proportional to the zero-width and aperture of the array. Therefore, [24] proposed a kind of zero-notch width that can be flexibly adjusted and can produce asymmetric zero-notch width to meet different situations. Since the antenna used on UAV is generally a two-dimensional array, we need the zero-trap broadening technology of a two-dimensional array. A null widening technique for the uniform circular array is proposed [25], but it is only limited to the broadening of the uniform circular array.

In this paper, based on Mailloux's zero-notch broadening method, a null widening method for two-dimensional arrays is proposed. The signal received by the drone's two-dimensional array antenna is determined by two dimensions of information. When adding a virtual interference source, you need to add a virtual interference source of equal interval and equal intensity in two dimensions. To produce asymmetrical and flexible zero-notch width, we increase the number of virtual interference sources near the interference signal asymmetrically. The method proposed in this paper can not only obtain a wide zero-trap width and flexibly adjust the width but also produce asymmetric width for the deviation of UAV jamming signal in practice, which does not need to cover the worst deviation to reduce the consumption of freedom. In the realization of zero-trap broadening, the performance of adaptive beamforming is seriously degraded due to the model adaptation in high SNR due to the inclusion of desired signals. In this paper, a sparse covariance matrix reconstruction method [18] is proposed to remove the desired signal information. Finally, given the problem that UAV may encounter in practice in accepting signals from multiple directions, this paper proposes to adopt a linear constrained minimum variance criterion (LCMV) [25] to form a multibeam direction graph. Finally, we simulate a concentric ring array, and the results show that the mismatch problem can be solved well in high SNR, and the asymmetric zero-trap width can be adjusted flexibly.

Section 2 introduces the basic signal model, Section 3 presents the sparse covariance matrix reconstruction method and the zero-trap spreading technique proposed in this paper, Section 4 presents the model of the concentric circular array and gives some simulation results, and finally, Section 5 gives our conclusions.

2. The Signal Model

2.1. Array Signal Model. Assume that signals emitted from radiation sources at far-field sources include the desired signal with direction θ_0 and M narrowband interference signals with direction $\theta_k(k = 1, 2, \cdots, M)$ and the inevitable noise signal. The array signal model is at this point [26].

$$X(t) = \mathrm{AS}(t) + n(t), \tag{1}$$

where $S(t) = [s_0(t), s_1(t), \cdots, s_M(t)]^T$ is the complex envelope of the received signal including desired signal and interfering signals, $n(t) = [n_1(t), n_2(t), \cdots, n_M(t)]^T$ is the noise that exists during transmission, $A = [a(\theta_0), a(\theta_1), \cdots, a(\theta_M)]$ is a matrix of the steering vectors corresponding to the above signal, and $(\cdot)^T$ is the transpose operation of a matrix. The steering vector [26] is

$$a(\theta) = \left[1, e^{j2\pi d \cos\theta/\lambda}, \cdots, e^{j2\pi(M-1)d \cos\theta/\lambda}\right]^T, \tag{2}$$

where λ is the operation wavelength and d is the distance between elements of the array generally taken as $\lambda/2$. The adaptive beamformer output is given by

$$y(t) = w^H X(t) = s(t) w^H a(\theta), \tag{3}$$

where $w = [w_1, w_2, \cdots, w_M]^T$ is the weight of the beamforming, and the weight is an important parameter in adaptive beamforming, and $X(t) = [x_1(t), x_2(t), \cdots, x_M(t)]^T$ is the signal accepted by each array element. $(\cdot)^H$ is the conjugate transpose operator symbol. To btain weights, the minimum variance distortion response (MVDR) beamforming problem is usually used [27].

$$\begin{cases} \min\limits_{w} w^H R_{i+n} w, \\ \text{s.t} w^H a(\theta_0) = 1, \end{cases} \tag{4}$$

and the solution is the MVDR beamformer, also referred to as the Capon beamformer. Then, the weights are given by

$$w_{\text{opt}} = \frac{R_{i+n}^{-1} a(\theta_0)}{a^H(\theta_0) R_{i+n}^{-1} a(\theta_0)}, \tag{5}$$

where R_{i+n} is the interference plus noise covariance matrix. In the real system, we cannot obtain the ideal covariance matrix, so the Sampled Covariance Matrix Inverse (SMI) algorithm is used, and the maximum likelihood estimation method is used to estimate the covariance matrix as $\widehat{R}_x(M) = 1/M \sum_{i=1}^{M} X(t_i) \mathrm{X}^H(t_i)$. Then, the weights of the SMI algorithm are expressed as $w_{\text{smi}} = \widehat{R}_x^{-1} a(\theta_0) / a^H(\theta_0) \widehat{R}_x^{-1} a(\theta_0)$. Since the SMI algorithm estimates the interference plus noise covariance matrix from the sampled signal, there must be information about the desired signal in it.

For a smooth random signal, the interference plus noise covariance matrix can be obtained based on its output signal power as

$$R_{i+n} = \sum_{l=1}^{L} \sigma_l^2 a(\theta_l) \mathrm{a}^H(\theta_l) + \sigma_n^2 \mathrm{I}. \tag{6}$$

2.2. Interference-Plus-Noise Covariance Matrix Reconstruction. Generally, the number of interference sources and their actual steering vectors and power are usually unknown. In addition, the noise power is also unknown. Therefore, to reconstruct the interference plus noise covariance matrix, we need to know the spatial-spectral distribution in all possible directions. In this correspondence, we use the Capon spatial spectrum estimator

$$\widehat{P}(\theta) = \frac{1}{a^H(\theta) \widehat{R}^{-1} a(\theta)}. \tag{7}$$

By substituting back the optimal weights of the MVDR beamformer, the objective function in its problem yields $\widehat{R}$. The covariance matrix of the disturbance plus noise can be reconstructed using the method of Capon's spectral estimation as

$$\tilde{R}_{i+n} = \int_{\Theta} \widehat{P}(\theta) a(\theta) a^H(\theta) d\theta = \int_{\Theta} \frac{a(\theta) a^H(\theta)}{a^H(\theta) \widehat{\mathrm{R}}^{-1} a(\theta)} d\theta, \tag{8}$$

where Θ is the range $\tilde{\Theta}$ that contains the interfering and noisy signals obtained by removing the desired signal that we can estimate. And their concatenation is the whole spatial domain, and their intersection is the empty set.

2.3. Regular Covariance Matrix Tapers. The method of covariance matrix taper, also known as the Mailloux–Zatman (MZ) null widening method, is achieved by modifying the original covariance matrix as follows:

$$\widehat{R}_{\text{MZ}} = \widehat{R} \circ T_{\text{MZ}}, \tag{9}$$

where T_{MZ} is a positive definite matrix of real numbers, where $\circ$ is the Hadamard product operation, which is the multiplication of the corresponding elements of two matrices.The cone operation on the covariance matrix is also called a cone matrix, and the corresponding elements of its mnth term are

$$[T_{\text{MZ}}]_{mn} = \sin c\left(\frac{(m-n)\Delta}{\pi}\right), \tag{10}$$

where Δ is the normalized virtual bandwidth by whose size and the width of the zero trap can be varied.

2.4. Multibeam Formation Algorithm. The LCMV criterion is a generalization of the MVDR criterion with the addition of multiple constraints. Assuming that the desired signal arrives in multiple directions at this time, we can obtain the basic mathematical model of the LCMV criterion as

$$\begin{cases} \min\limits_{w} w^H R_x w, \\ \text{s.t} w^H C = F^H. \end{cases} \tag{11}$$

According to equation (11), we can then obtain the optimal weights under the LCMV criterion as

$$w_{\text{opt}} = {R_x}^{-1} C \left(C^H {R_x}^{-1} C\right)^{-1} F, \tag{12}$$

where $F^T = [c_1, c_2, \cdots, c_L]$ is a vector of constants in dimension $L \times 1 (L \geq 1)$. The constant value c is generally taken as 1, and $C = [a(\theta_0), a(\theta_1), \cdots, a(\theta_{L-1})]$ is the popularity matrix of the A-dimensional oriented vector.

3. The Proposed Algorithm

3.1. Interference-Plus-Noise Covariance Matrix Sparse Reconstruction. In array signal processing, generally, the number of signals sent by the array accepting radiation sources is much smaller than the number of array elements. That is, the sources are sparse in the observation field. In this case, the reconstruction of the (6) covariance matrix does not need to be integrated over the entire airspace coverage. Thus, sparsity can be exploited to

Table 1: Parameters of concentric seven circles.

	Circle 1	Circle 2	Circle 3	Circle 4	Circle 5	Circle 6	Circle 7
Radius (m)	$\lambda/2$	λ	$3\lambda/2$	4λ	$5\lambda/2$	6λ	$7\lambda/2$
Number	7	13	19	26	32	38	44
Angle (rad)	$2\pi/7$	$2\pi/13$	$2\pi/9$	$\pi/13$	$\pi/16$	$\pi/19$	$\pi/22$

reconstruct the covariance matrix. The sparse constrained optimization problem used to determine the source location and its power is obtained by combining the l_0-norm (denoted by $\|.\|_0$) and can be expressed as

$$\min_{P,\sigma_n^2} \left\|\widehat{\mathrm{R}}_x - APA^H - \sigma_n^2 I\right\|_F^2 + \gamma\|p\|_0, \quad \text{subject to } p \geq 0, \sigma_n^2 > 0, \tag{13}$$

where p is the spatial spectrum of the signal we wish to obtain over the entire range of signal space, P is the diagonal matrix of p, $A = [a(\theta_1), a(\theta_2), \cdots, a(\theta_N)]$ is an array of streamlined matrices, σ_n^2 is the noise power taken as the minimum eigenvalue of the covariance matrix, I is an identity matrix, γ controls the tradeoff between the sparsity of the spectrum and the residual norm, and $\|.\|_F$ is the Frobenius norm of a matrix. The optimization problem (13) is a CS problem. This is a difficult combinatorial optimization problem, but when the problem is sparse enough, we can turn it into a l_1-norm (denoted by $\|.\|_1$) problem. Assuming that the DOA estimate of the desired signal is already known, the problem (13) degenerates to an inequality constrained least squares problem. Thus, (13) can be simplified as

$$\min_{p\left(\widetilde{\theta}_p\right)} \left\|\widehat{R}_x - \widehat{\sigma}_n^2 I - A\left(\widetilde{\theta}_p\right) P\left(\widetilde{\theta}_p\right) A^H\left(\widetilde{\theta}_p\right)\right\|_F^2, \quad \text{subject to } p\left(\widetilde{\theta}_p\right) > 0, \tag{14}$$

where $\widetilde{\theta}_p$ is the direction of the signal for which we want to estimate the spatial spectrum. This is a convex optimization problem [28, 29] and can be solved using convex optimization software [30]. There are only Q nonzero results in the derived result, and based on the spatial spectrum of Q-sparse, we can reconstruct the interference plus noise covariance matrix

$$\tilde{R}_{i+n} = \sum_{k=1_{k\neq q}}^{Q} p\left(\widetilde{\theta}_{p_k}\right) a\left(\widetilde{\theta}_{p_k}\right) a^H\left(\widetilde{\theta}_{p_k}\right) + \widehat{\sigma}_n^2 I. \tag{15}$$

Thus, we can obtain the weights of the adaptive beamformer based on the covariance matrix reconstruction as

$$w = \frac{\tilde{R}_{i+n}^{-1} a(\theta_0)}{a^H(\theta_0)\tilde{R}_{i+n}^{-1} a(\theta_0)}. \tag{16}$$

3.2. Null Broadening with Covariance Matrix Reconstruction in 2D Arrays. We know that the expansion matrix T_{MZ} in (9) is the well-known Mailloux or Zatman method. We use the example based on Mailloux's idea, which is to assume the existence of a set of virtual disturbances around narrowband disturbances. Firstly, in a 1D array, we can obtain the mnth term of the covariance matrix using Mailloux's method as

$$\tilde{R}_{mn} = [R]_{mn} \cdot \sin c\left[\frac{(m-n)dW}{\lambda}\right] = [R]_{mn} \cdot [T_{\mathrm{MZ}}]_{mn}, \tag{17}$$

where T_{MZ} is the tapered matrix. To be able to generate asymmetric zero traps, replace the equally spaced virtual interference range in the vicinity of the disturbance in the Mailloux method with $-I_1$ to I_2. Thus, the tapered matrix T can be obtained

$$\left[\tilde{T}_{\mathrm{MZ}}\right]_{m,n} = \sin c\left(\frac{(m-n)(W_2+W_1)d}{\lambda}\right) \cdot e^{j\pi d(m-n)(W_2-W_1)/\lambda}, \tag{18}$$

where W_1 and W_2 are the widening factors, and the size of which can be adjusted to obtain asymmetric zero-trap widths on each side of the interference. In a two-dimensional array, the direction of origin of the signal is determined by the azimuth θ and pitch angles φ, where the steering vector is

$$\mathrm{a}(\theta,\varphi) = \begin{bmatrix} 1 \\ e^{j(2\pi d/\lambda)\cdot L_1 \cdot B_{\theta,\varphi}} \\ \vdots \\ e^{j(2\pi d/\lambda)\cdot L_{M-1} \cdot B_{\theta,\varphi}} \end{bmatrix}, \tag{19}$$

where $B_{\theta,\varphi} = (\cos\theta \sin\varphi, \sin\theta \sin\varphi)^T$ and L is the coordinate of the all array element of the two-dimensional array. The expression for the covariance matrix of interference plus noise is obtained by substituting the steering vector of the 2D array

$$R_{i+n} = \sum_{i=1}^{Q} \sigma_I^2 a(\theta_i,\varphi_i) a^H(\theta_i,\varphi_i) + \widehat{\sigma}_n^2 I. \tag{20}$$

According to the idea of the Mailloux method, in a one-dimensional array, since the signal emitted by the source is accepted as equivalent to a plane wave, we only

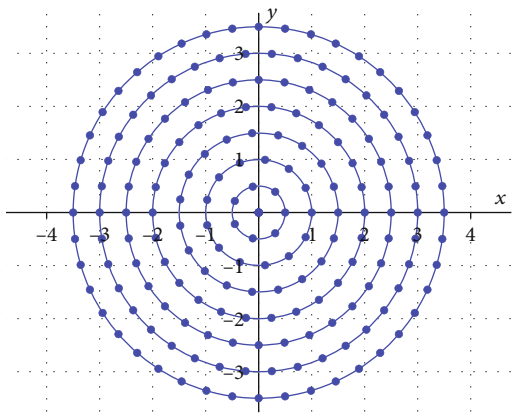

FIGURE 1: Schematic diagram of the concentric seven-circle array model.

need to add equally spaced virtual interference in one dimension to broaden the zero trap. However, in a two-dimensional array, the signal may be received from all angles in space, and its direction is determined by two angles, the azimuth θ and pitch angles φ, so it is necessary to add virtual interference in two dimensions to form the zero trap.

To derive the tapered matrix for the zero-trap spread of a two-dimensional array, we need to consider the coordinates of the array elements of the two-dimensional array when calculating the covariance matrix. Then, the coordinate matrix of the M array elements is expressed as

$$L = \begin{bmatrix} x_0 & y_0 \\ x_1 & y_1 \\ \vdots & \vdots \\ x_{M-1} & y_{M-1} \end{bmatrix}, \tag{21}$$

where (x, y) is the coordinate of each array element of the two-dimensional array. By substituting the coordinate values into the calculation of the steering vector, we obtain the steering vector as

$$a(\theta, \varphi) = \begin{bmatrix} 1 \\ e^{j2\pi d(x_1 u + y_1 v)/\lambda} \\ \vdots \\ e^{j2\pi d(x_{M-1} u + y_{M-1} v)/\lambda} \end{bmatrix}, \tag{22}$$

where $u = \cos\theta \sin\varphi$ and $v = \sin\theta \sin\varphi$. According to equation (24) we know that the interference-plus-noise covariance matrix R_{i+n} is actually the guided vector multiplied by its transpose matrix, that is, each term of the covariance matrix $[\mathrm{R}_{i+n}]_{mn}$ is actually the product of the mth term of a column vector and the nth term of its conjugate transposed row vector, so the mnth term of the covariance matrix can be obtained as

$$\begin{aligned} [R_{i+n}]_{mn} &= \sum_{q=1}^{Q} \sigma_q^2 e^{j2\pi d(x_m u + y_m v)/\lambda} \\ &\cdot \sum_{q=1}^{Q} \sigma_q^2 e^{-j2\pi d(x_n u + y_n v)/\lambda} \\ &= \sum_{q=1}^{Q} \sigma_q^2 e^{j2\pi d[(x_m - x_n)u + (y_m - y_n)v]/\lambda}, \end{aligned} \tag{23}$$

where σ_q^2 is the power of the qth interfering signal. To widen the zero-trap width at the suppressed disturbances, we need to add J equally spaced virtual disturbances in the x and y coordinate dimensions, respectively. Then, the $[\tilde{R}_{i+n}]_{mn}$ equation is expressed as

$$\begin{aligned} \left[\tilde{R}_{i+n}\right]_{mn} &= [R_{i+n}]_{mn} \cdot \sin c\left[\frac{(x_m - x_n)dW_x}{\lambda}\right] \cdot \sin c \\ &\cdot \left[\frac{(y_m - y_n)dW_y}{\lambda}\right] = [R_{i+n}]_{mn} \cdot [T_{PA}]_{mn}, \end{aligned} \tag{24}$$

where T_{PA} is a two-dimensional planar array of zero-trapped widened tapered matrices. Thus, we can then obtain the mnth term of the tapering matrix of the zero-trap spread of the two-dimensional array as

$$\begin{aligned} [T_{PA}]_{mn} &= \sum_{p_x=-(J-1)/2}^{(J-1)/2} e^{j2\pi d[(x_m - x_n)p_x \Delta u y \lambda} \cdot \sum_{p_y=-(J-1)/2}^{(J-1)/2} e^{j2\pi d} \\ &\cdot \left[(y_m - y_n)p_y \Delta u\right]/\lambda = \sin c\left[\frac{(x_m - x_n)dW_x}{\lambda}\right] \cdot \sin c \\ &\cdot \left[\frac{(y_m - y_n)dW_y}{\lambda}\right]. \end{aligned} \tag{25}$$

When we use two-dimensional array elements to receive signals may not need to spread the same width at the same time at the interference, which requires us to have the flexibility to adjust the width, we make the equally spaced interference from $-J_1$ to J_2 in x dimension and from $-J_3$ to J_4 in y dimension, and then, the tapering matrix is modified as

$$\begin{aligned} \left[\tilde{T}_{PA}\right]_{mn} &= \sum_{p_x=-J_1}^{J_2} e^{j2\pi d[(x_m - x_n)p_x \Delta u]\lambda} \cdot \sum_{p_y=-J_3}^{J_4} e^{j2\pi d\left[(y_m - y_n)p_y \Delta u\right]\lambda = \sin c\left((x_m - x_n)\left(W_{x2} + W_{x1}\right)d/\lambda\right)} \\ &\cdot e^{j\pi d(x_m - x_n)\left(W_{x2} - W_{x1}\right)/\lambda \cdot \mathrm{sinc}\left((y_m - y_n)\left(W_{y4} + W_{y3}\right)d/\lambda\right) \cdot e^{j\pi d(y_m - y_n)\left(W_{y4} - W_{y3}\right)/\lambda}}, \end{aligned} \tag{26}$$

where $J_1 \Delta u = W_{x_1}$, $(J_2 + 1)\Delta u = W_{x_2}$, $J_3 \Delta u = W_{y_3}$, $(J_4 + 1)\Delta u = W_{y_4}$. Equation (26) is an asymmetric two-dimensional array of tapered matrices, and it can not only expand the space for the zero trap but also offset the phase.

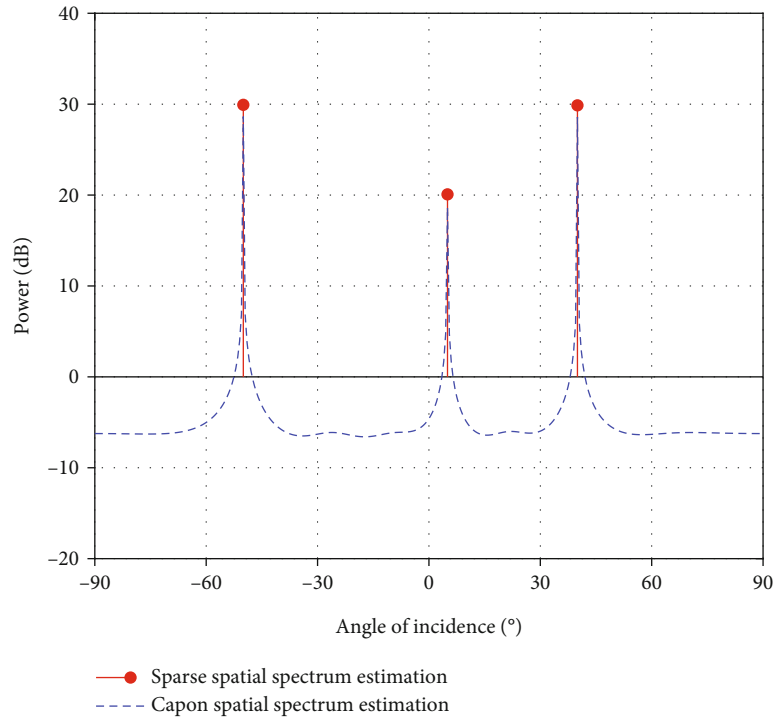

Figure 2: Comparison of sparse spatial spectrum estimation and Capon spatial spectrum estimation.

3.3. Concentric Circle Array Model. The concentric ring array consists of a central array element and N circles of concentric rings, with the number of circles set according to requirements. The radius of the ith concentric ring is taken as the half-wavelength multiplied by the number of turns ith which is

$$r_i = \frac{\lambda}{2} \cdot i(i = 1, 2, \cdots, N). \tag{27}$$

The spacing of the array elements on the circle should meet the arc length between two adjacent array elements should be less than or equal to half a wavelength as

$$\frac{2\pi r_i}{k_i} \leq \frac{\lambda}{2} \Rightarrow k_i \geq 2\pi i. \tag{28}$$

Since the number of elements is an integer, we round up to get the number of elements on the ith circle as

$$k_i = \lceil 2\pi i \rceil, \tag{29}$$

where $\lceil \cdot \rceil$ is an upward rounding symbol. Since the array elements on each circle are uniformly equidistant from each other, we can obtain the corresponding angle between the arc lengths of each array element as

$$\alpha_i = \frac{2\pi}{k_i}. \tag{30}$$

Thus, we can get the coordinates of each array element as

$$\begin{cases} x_{k_i} = r_i \cos \alpha_i, \\ y_{k_i} = r_i \sin \alpha_i. \end{cases} \tag{31}$$

In this paper, the concentric seven-ring array model is used, and the corresponding parameters of the array are calculated as shown in Table 1, and the schematic diagram of the array model is shown in Figure 1.

4. Simulation

4.1. Interference-Plus-Noise Covariance Matrix Sparse Reconstruction. In the simulation, a uniform line array model with 10 arrays is considered, the desired signal from 5° directions with a signal-to-noise ratio of 15 dB, interference from -50° and 40° with a signal-to-noise ratio of 30 dB, and the number of sampling snapshots used in the simulation is 300.

A comparison plot of Capon spectral estimation and sparse spectral estimation is shown in Figure 2. From Figure 2, we can see that the spectrum obtained from Capon spectral estimation has valued over the whole range and high spikes at the estimated interference and at the desired signal, while the spectrum obtained from sparse spectral estimation only has an impulse at the interference and at the desired signal with zero values in the other directions. This means that sparse spectral estimation can provide a good estimate of the location and power of our signal of interest.

Figure 3 shows the directional diagram for different methods at a signal-to-noise ratio of 15 dB. We can see that

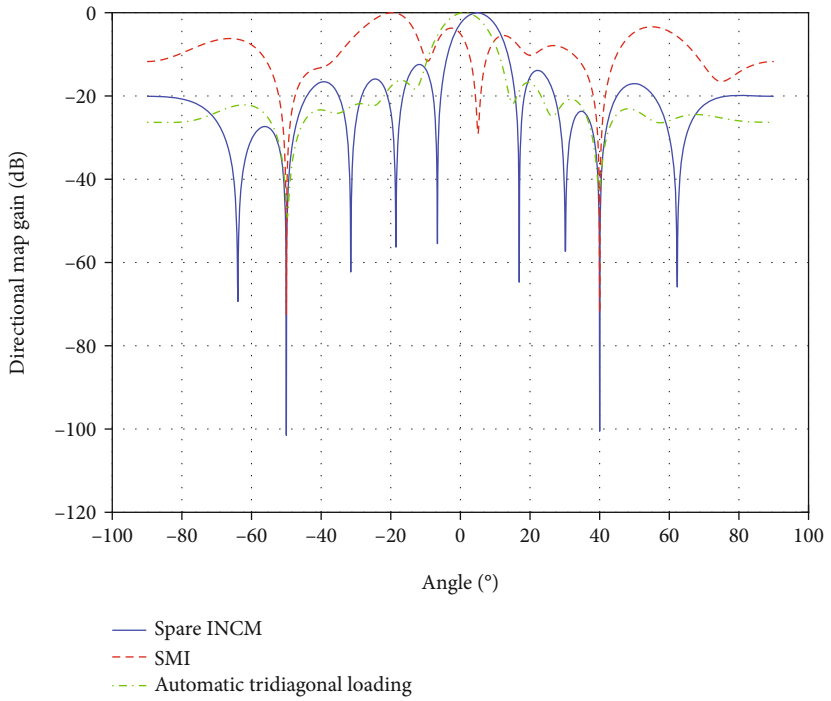

Figure 3: Diagram for different methods at a signal to noise ratio of 15 dB.

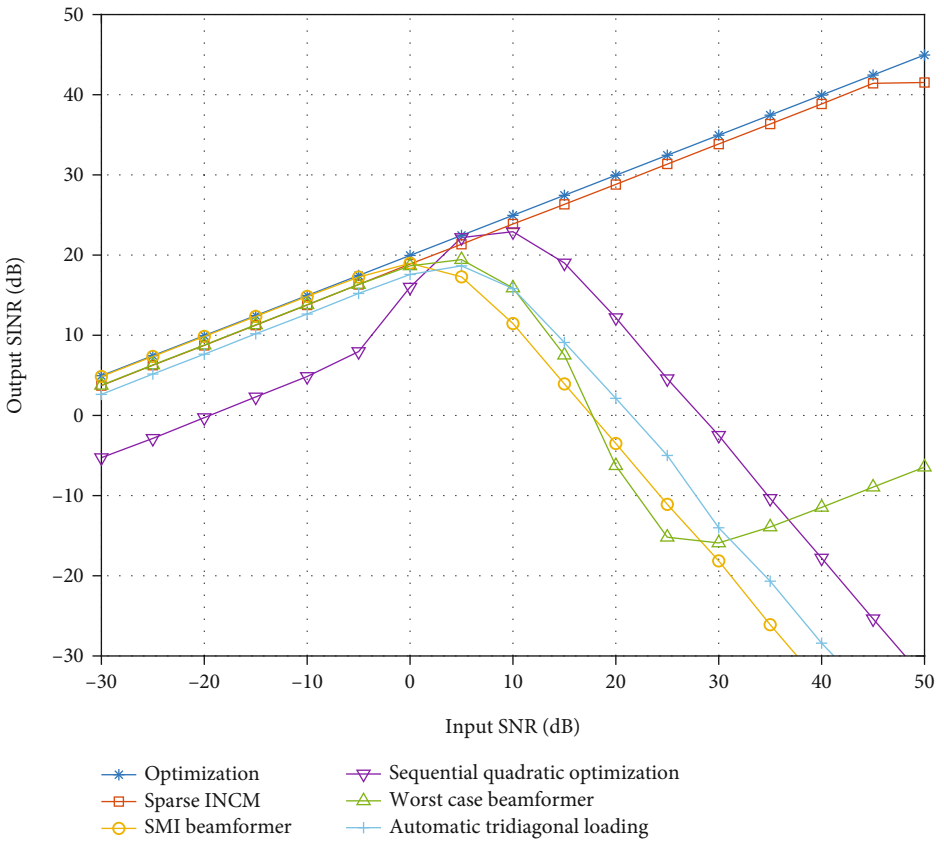

Figure 4: The effect of input SNR on output SINR.

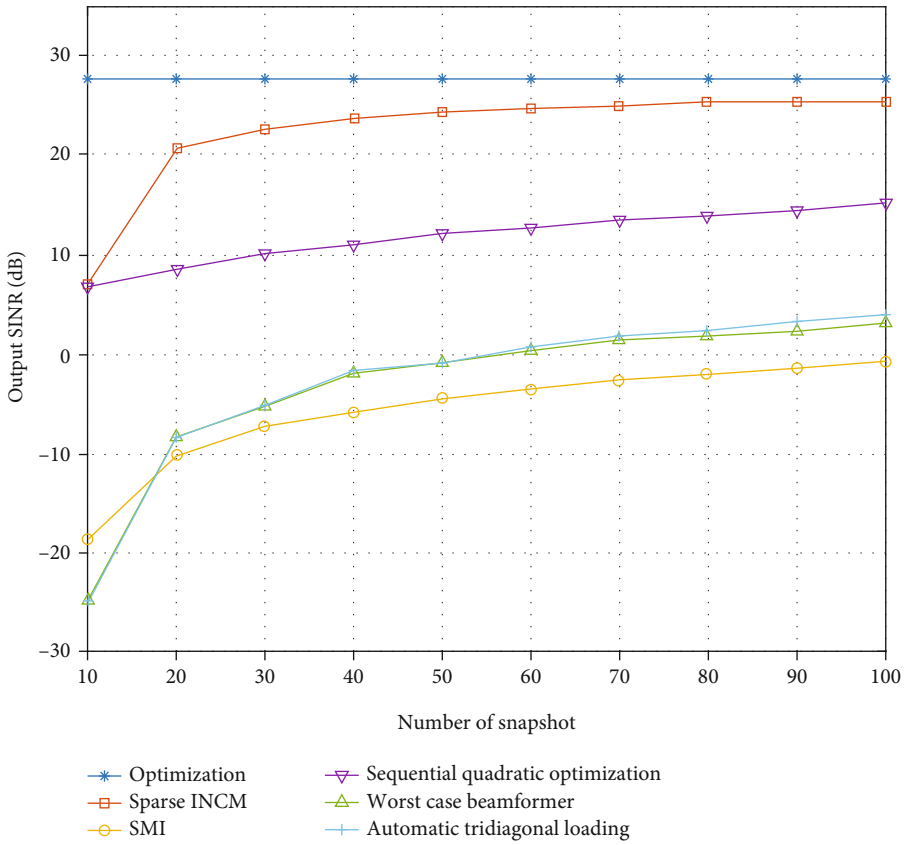

Figure 5: The effect of number of sampling snapshots on output SINR.

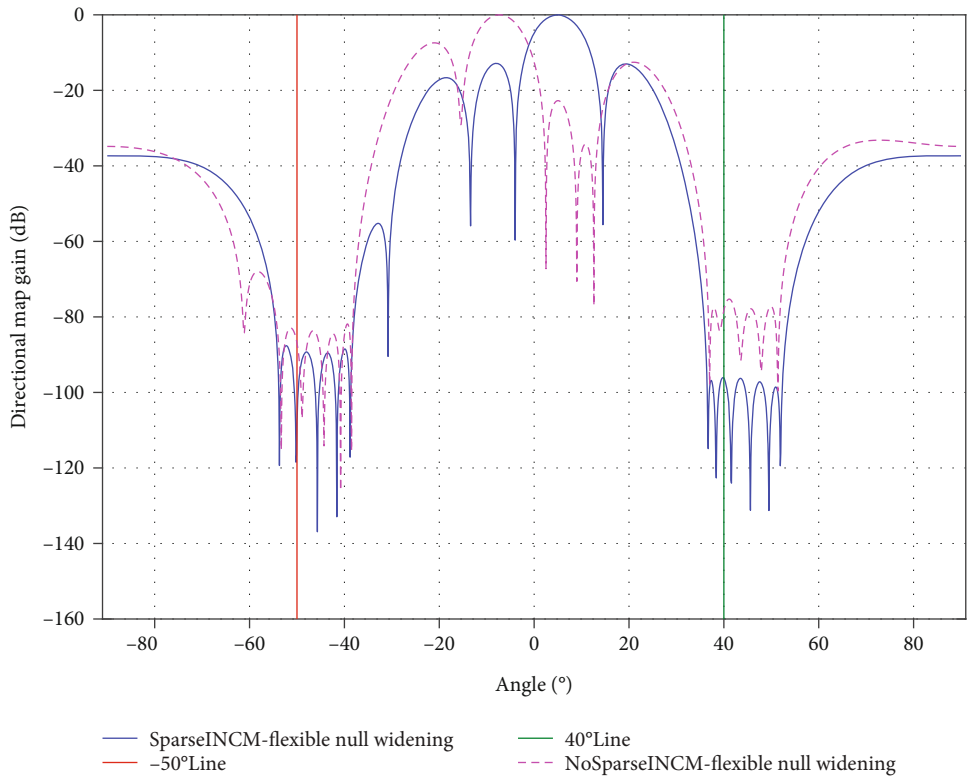

Figure 6: Comparison of flexible nulling widening with and without sparse INCM.

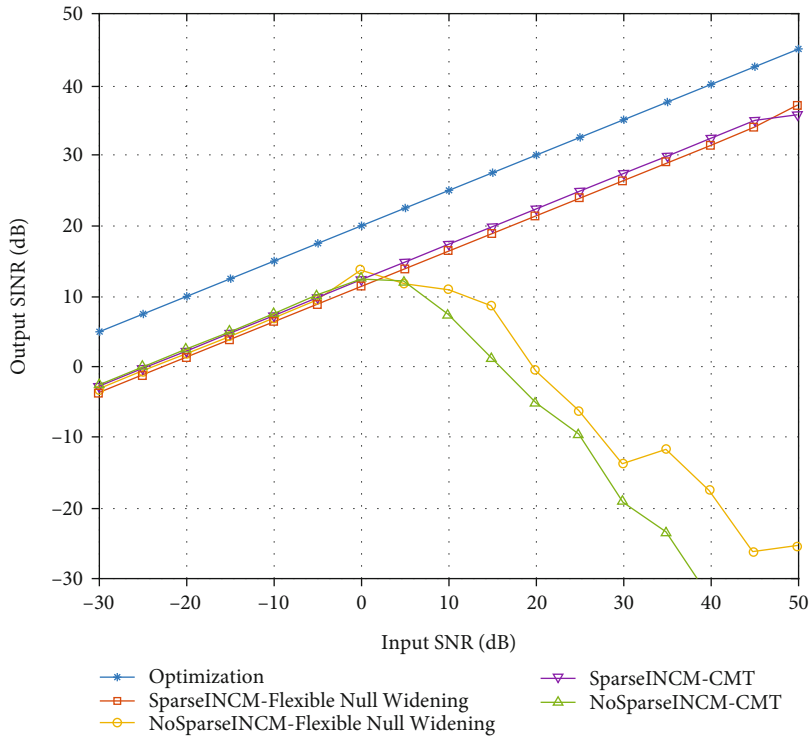

Figure 7: Null widening at INCM, for input SNR on output SINR.

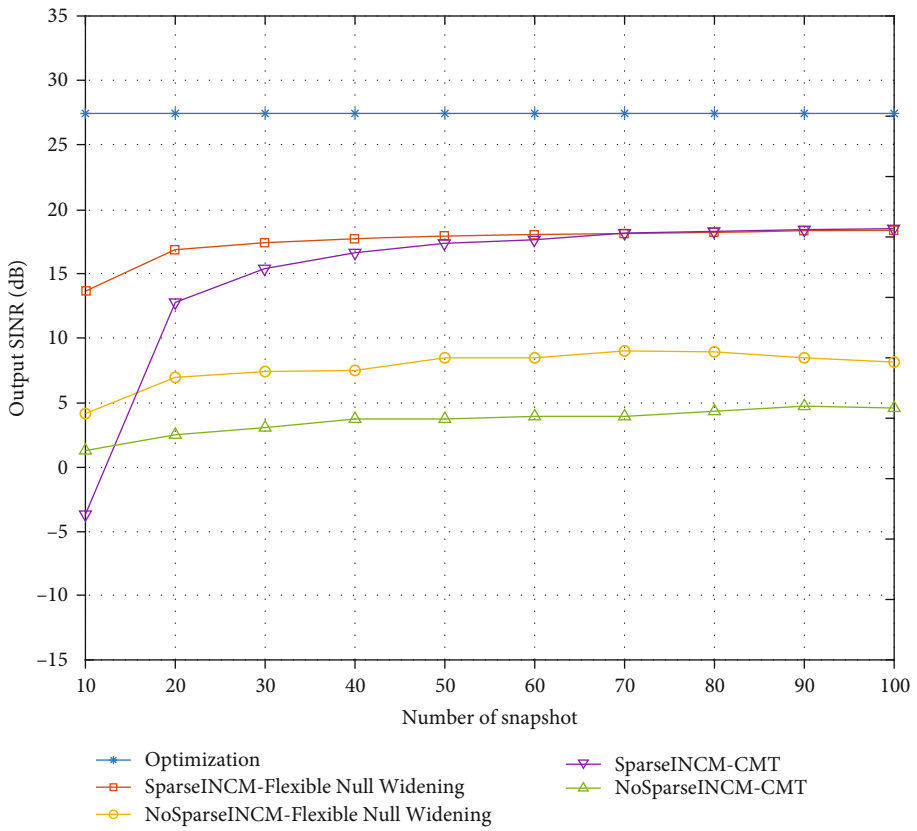

Figure 8: Null widening at INCM for number of sampling snapshots on output SINR.

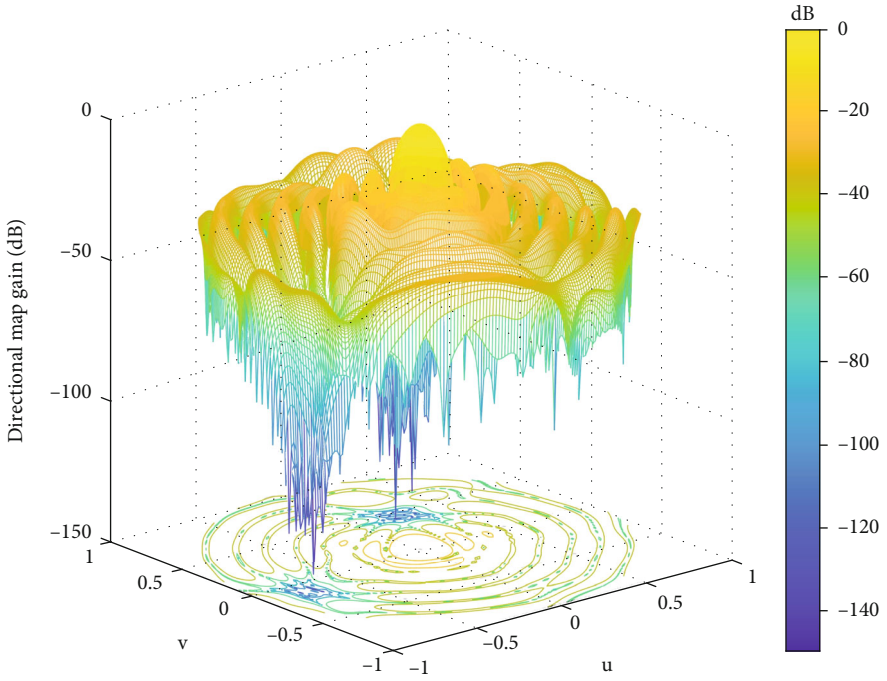

(a) 3D orientation diagram

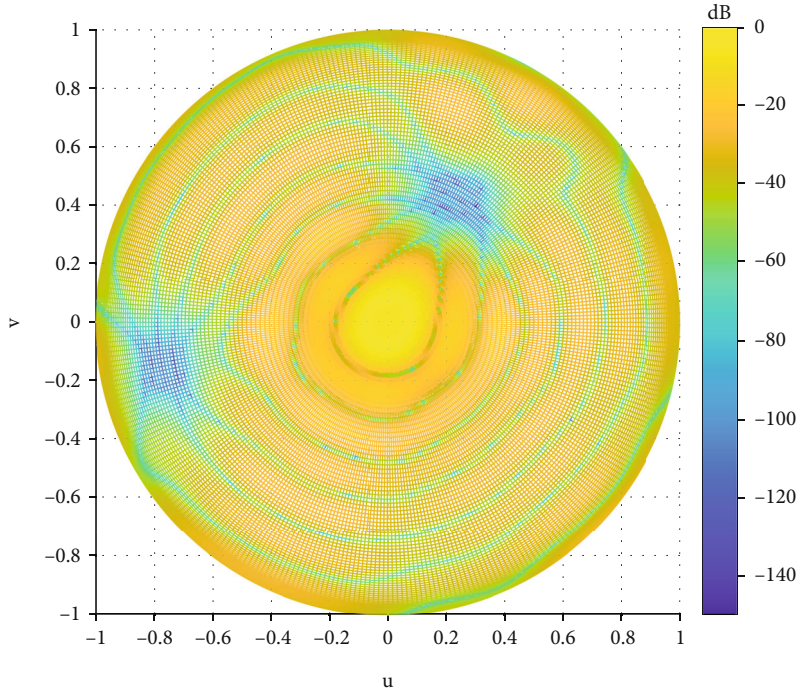

(b) Top view

Figure 9: Continued.

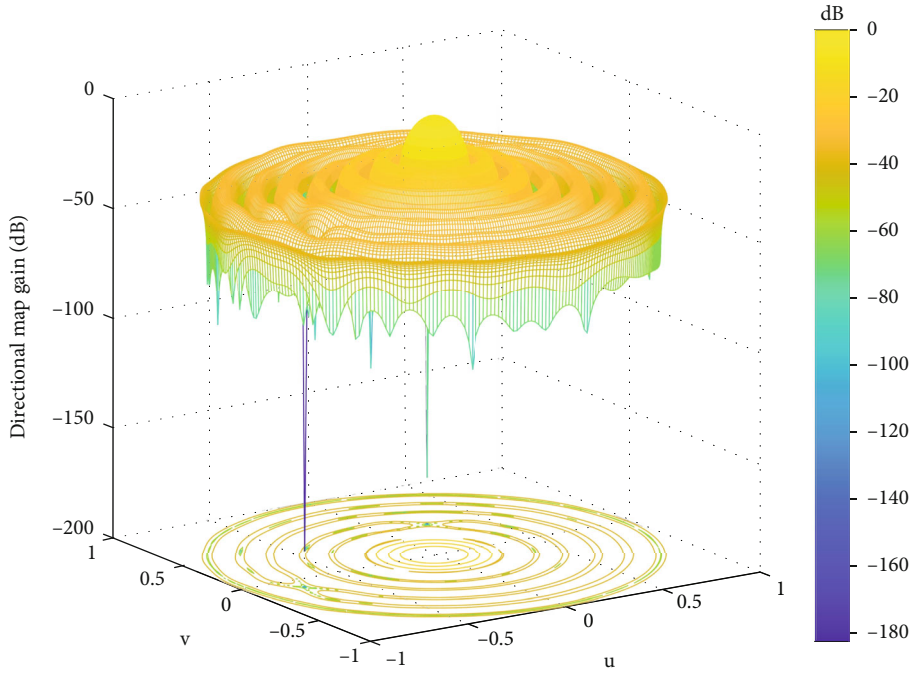

(c) 3D orientation diagram without widening

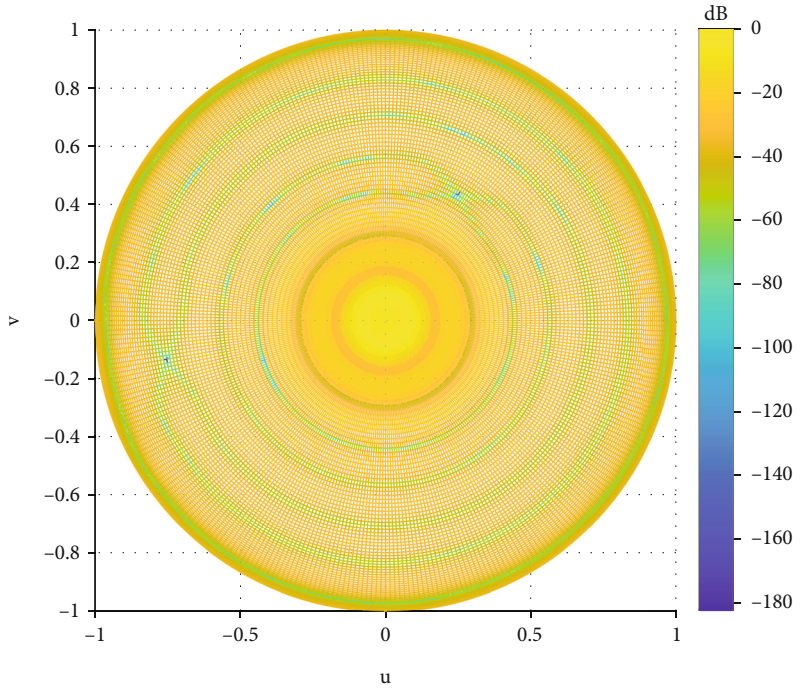

(d) Top view without widening

Figure 9: Orientation diagram of the concentric circle.

at large signal-to-noise ratios, the SMI algorithm [12] obtains a directional map with a significant mismatch that does not form the main beam gain. In contrast, sparse interference-noise covariance matrix reconstruction (INCM) [18] gives a stable directional map with good gain in the main beam direction and a deep zero trap against interference. In addition, we also compare an automatic tri-diagonal loading method [15], which also produces a gain in the main beam but has a wider dominant flap and is much less suppressive of interference than the sparse INCM method [18].

The effect of the input signal-to-noise ratio on the output signal-to-noise ratio is shown in Figure 4, where the input signal-to-noise ratio ranges from -30 dB to 50 dB. We

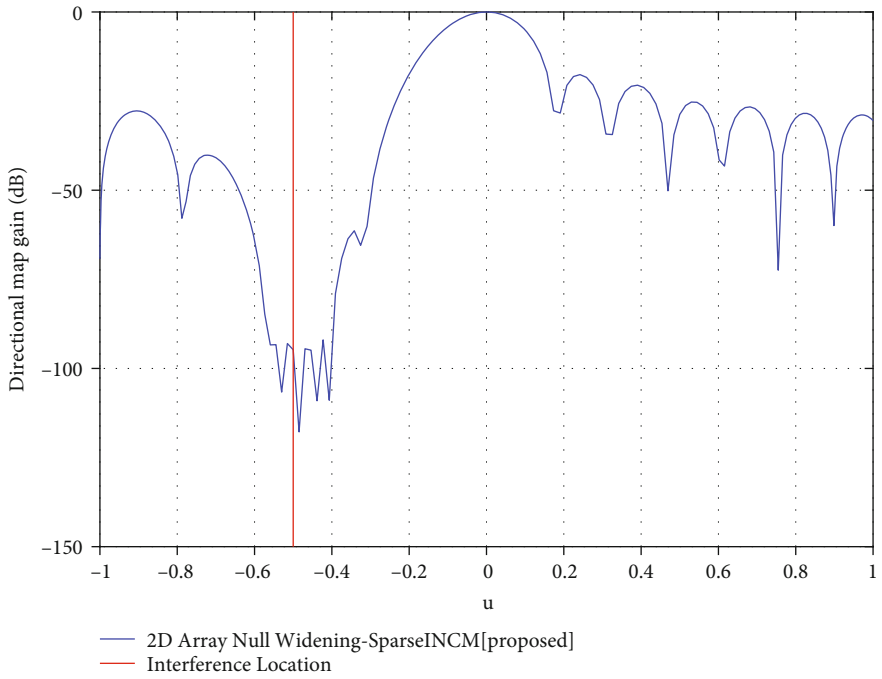

(a) Spread width at $\theta = 60\circ, \varphi = 30\circ$

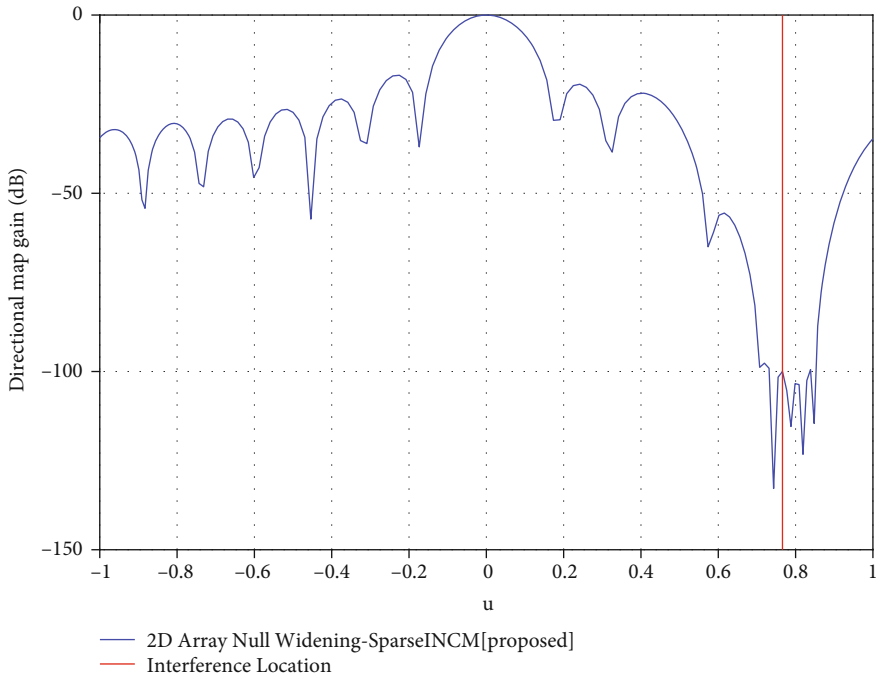

(b) Spread width at $\theta = 190\circ, \varphi = 50\circ$

Figure 10: Continued.

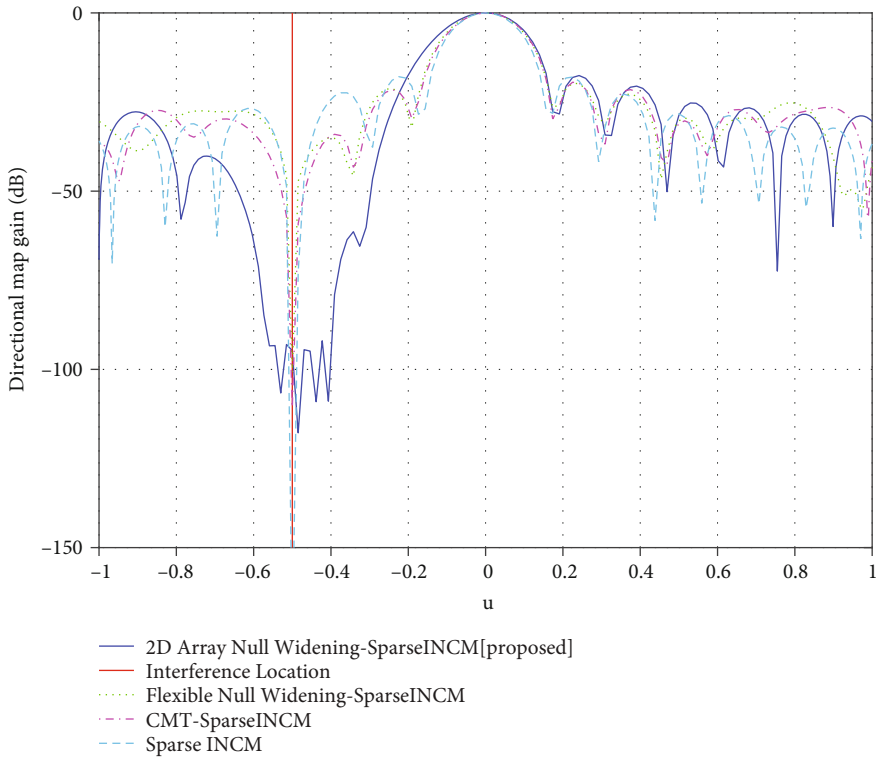

(c) Contrast unexpanded at $\theta = 60\circ, \varphi = 30\circ$

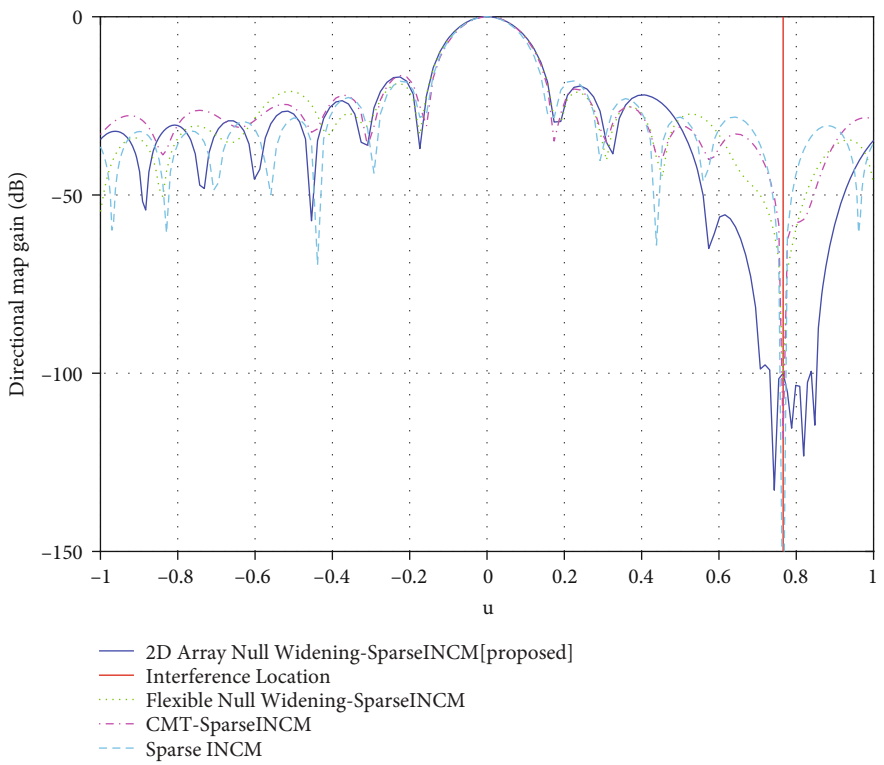

(d) Contrast unexpanded at $\theta = 190\circ, \varphi = 50\circ$

Figure 10: Cross-sectional view at two disturbances.

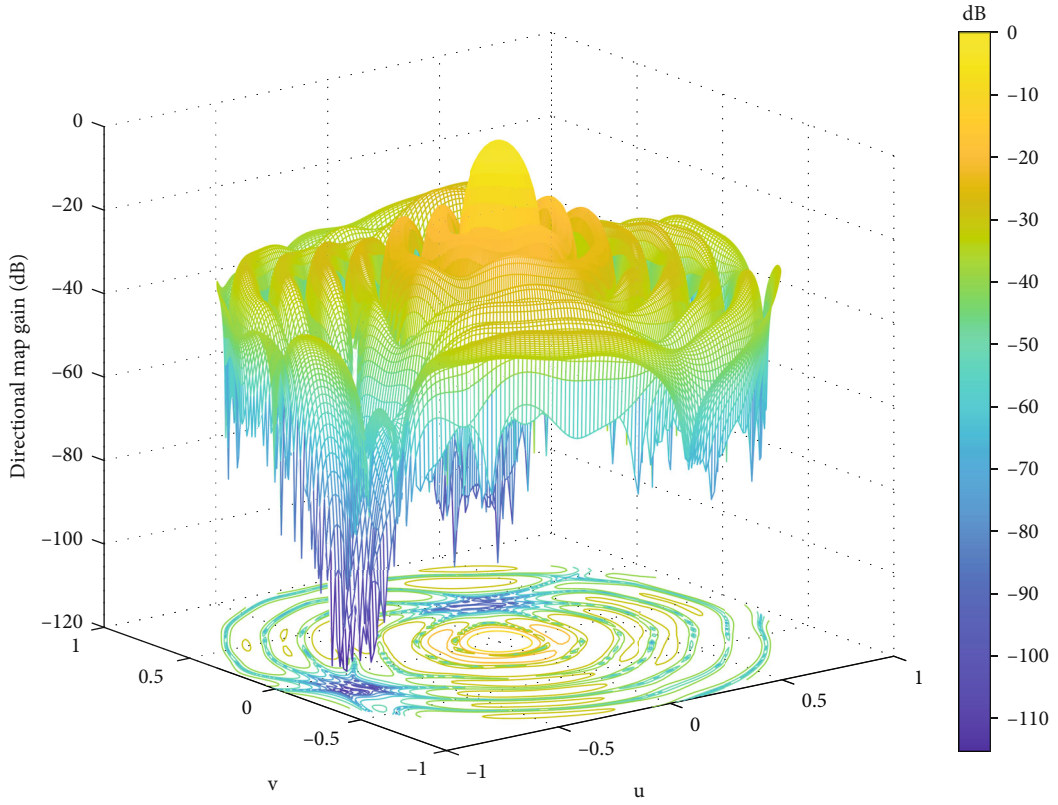

(a) SNR = −10 dB

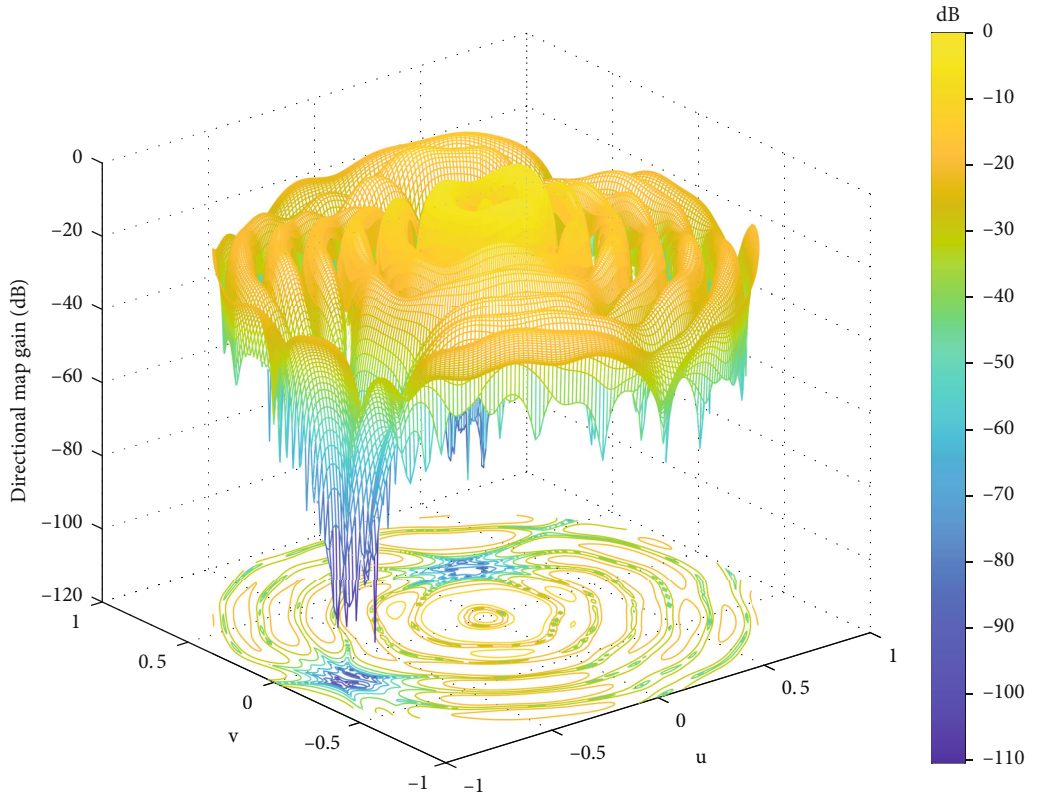

(b) SNR = 10 dB

Figure 11: Directional map of the SMI algorithm to calculate the covariance matrix.

compare the sparse INCM [18] with several methods including the automatic tridiagonal loading method [15], sequential quadratic beamforming [16], worst-case beamforming [14], the basic SMI algorithm [12], and optimal beamforming without model mismatching. It shows that at low signal-to-noise ratios, the output SINR of the other methods is essentially the same, but as the input signal-to-noise ratio increases, there is an inflection point in the range of 0 dB to 10 dB where the performance starts to deteriorate.

In contrast, the sparse INCM method is not affected by the input signal-to-noise ratio. The effect of the number of sampling snapshots on output SINR is shown in Figure 5, with snapshots ranging from 10 to 100. We still compare several methods and see that the output SINR of the sparse INCM is significantly higher than that of the other methods. And it can be seen that the worst-case beamforming [14], automatic tridiagonal loading method [15], and the basic SMI algorithm [12] perform poorly at large SNRs. Their SINR is basically around 0 dB. Sequential quadratic beamforming [16] is more than 10 dB higher than them, but still more than 10 dB lower than the SINR under sparse INCM. The sparse INCM is basically close to the optimal value.

4.2. Flexible Null Broadening Technology in 1D Arrays. The simulation selects a uniform line array model with 16 elements, the desired angle of the signal is 5°, the corresponding signal-to-noise ratio is 15 dB, the interference signal is coming from the -50° and 40° direction, and its signal-to-noise ratio is 30 dB; the parameters of zero-trap width are set to $W_1 = 0.05$ and $W_2 = 0.15$.

The results of the simulation are shown in Figure 6. From the figure, we can see that the flexible zero-trap widening technique can produce asymmetric zero-trap widths to the left and right of the interference and can result in wider zero traps whether or not the sparse INCM [18] method is used. However, we can see that without the sparse INCM method, there is a clear mismatch in the directional map at large signal-to-noise ratios. With the latter method, not only a good main beam gain but also a deeper zero trap can be obtained.

In addition, we compared the results for the output SINR, using the same parameters for the desired signal as well as for the interference signal as in the directional diagram above and using 100 Monte Carlo experiments. The final result number of sampling snapshots and input signal-to-noise ratio on the output SINR is shown in Figures 7 and 8. In Figures 7 and 8, we compare the output SINR of the two methods using flexible nulling widening (FNW) [24] and covariance matrix tapered technique (CMT) [19] under sparse interference plus noise covariance matrix reconstruction as well as the conventional one. From Figure 7, we can see that as the input SNR increases, the output SINR is more or less the same at low SNR and the CMT and not. This is due to the Maxlloux method [21] of derivation in the FNW, which introduces noise along with virtual interference, so the output SINR is slightly worse. However, it is possible to produce asymmetric zero traps and to save degrees of freedom [23]. Similarly, from Figure 8, we can see that the output SINR of FNW and CMT with sparse INCM [18] is significantly higher as the number of samples

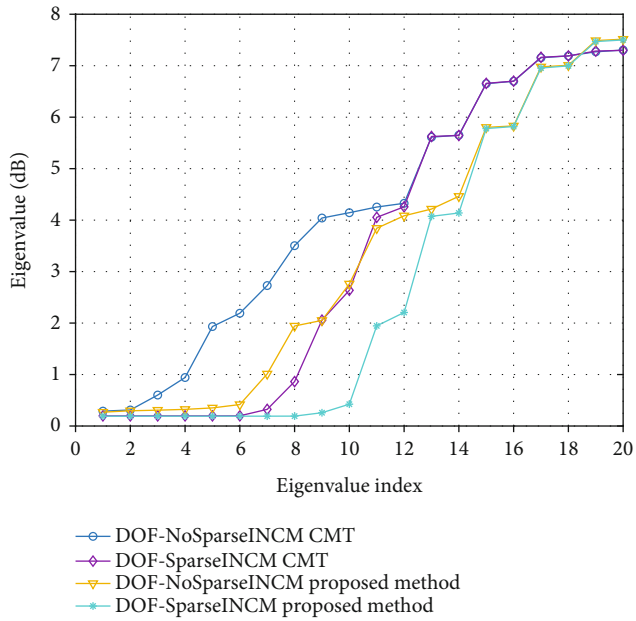

Figure 12: The DOF comparison between this method and the CMT method with and without the sparse INCM.

varies with the number of fast samples due to the result of not using it. Moreover, we can see that the two methods based on the sparse INCM converge in the end with an increasing number of beats. However, the results in both Figures 7 and 8 are worse than the optimal case without mismatch, because the other method introduces noise while spreading the zero trap, making the output SINR.

4.3. Null Broadening with Covariance Matrix Reconstruction in 2D Arrays. In this section of the simulation, the concentric circular array model of the seven rings mentioned in A is used to receive the signal with the relevant parameters as shown in Table 1. Assuming that the desired signal has an azimuth of 180°, a pitch angle of 0°, and a signal-to-noise ratio of 10 dB, there are two interfering signals with azimuths of 60° and 190°, pitch angles of 30° and 50°, and a signal-to-noise ratio of 30 dB. The number of sampling snapshots is chosen as 1024. The parameters of zero-trap width are set to $W_1 = 0.05$, $W_2 = 0.10$ and $W_3 = 0.05$, $W_4 = 0.1$. We use the $u - v$ coordinate system when forming the orientation diagram.

The 3D orientation of its simulation is shown in Figure 9(a), and its top view is Figure 9(b). In contrast, Figures 9(c) and 9(d) show the orientation diagrams of the concentric ring array without the zero-trap widening. It can be seen that our proposed method produces a significant width at the interference, whereas without widening, there is only a very narrow zero trap at the interference, which does not suppress the deviating signal well and thus reduces the UAV's immunity to interference when receiving signals.

Next, we have made a cross-sectional plot of Figure 10 for each of the two interference directions, and we can see that we have not only widened the zero trap at the

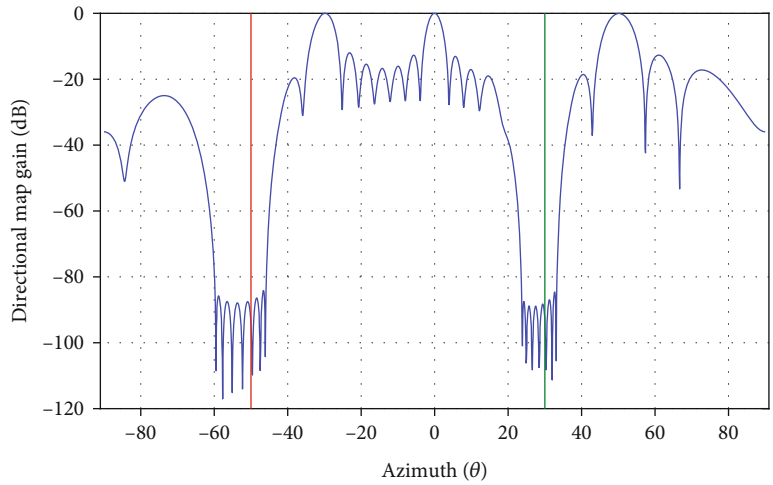

Figure 13: Directional map of multiple beamforming for a uniform line array of 32 array elements.

interference but also achieved a flexible asymmetric spreading for the width of the zero trap on both sides of the interference. We can clearly see from Figures 10(a) and 10(b) that our approach yields a wider zero trap and can produce different widths on each side of the interference, allowing the UAV to effectively suppress the deviating interference signal while the asymmetric width reduces the waste of degrees of freedom [22]. Figures 10(c) and 10(d) mainly compare several widening methods with the proposed method including CMT, FNW, and without valence, and we compare the zero-trap widths of several methods at different depths under the interference signal of $\theta = 60\circ, \varphi = 30\circ$ in Table 2. Here, the width is the u-coordinate as the metric. From the comparison of Figures 10(c) and 10(d) and the data in the table, we can see that although the CMT [19] and FNW [24] methods have a good effect in spreading the zero traps in 1D arrays, they are basically unable to widen the zero traps in 2D arrays, and even the depth of the zero traps is much reduced.

Table 2 shows that the depth and width of the zero traps in the two-dimensional arrays of methods [18, 23] are worse than the method proposed in this paper, while the zero traps that can be obtained by the method in this paper have a deeper depth and wider width. The proposed approach can not only cope with the spreading of zero traps in 2D arrays but can also take into account the depth of zero traps and still have a good spreading effect in deeper zero traps. The covariance matrices we use in the above process are all sparse INCM methods. However, if we use the ordinary SMI algorithm to obtain the covariance matrix, we can only form a good directional map at a low SNR such as Figure 11(a), where the expected signal direction is -10 dB, and when we increase the SNR to 10 dB, the directional map becomes Figure 11(b), which cannot form the main beam.

4.4. Analysis of DOF. Figure 12 shows a simulation comparing the degrees of freedom between the CMT and the widened zero-trap approach proposed in this paper and incorporating a comparison of the reconstructed interference plus noise covariance matrix and the degrees of freedom without reconfiguration. Here, we have used an array of 20 array elements. The flexible null widening method of the widening factor is $W_1 = 0.05$, $W_2 = 0.10$. The CMT has to cover the worst case, so the widening factor used is 0.2. It can be seen that in Figure 12, the asymmetric widening reduces about 4 DOF. And with the interference plus noise covariance matrix reconstruction, it can be reduced by about 4 DOF.

4.5. Multibeam Formation in 2D Arrays. This section simulates the LCMV-based multibeam directional map formation. Firstly, a 1D uniform line array is simulated, using a 32 array ULA array, with the desired signals from -30°, 0°, and 50°, whose signal-to-noise ratios are 8 dB, 10 dB, and 5 dB, respectively. Two interfering signals are from -50° and 30°, whose signal-to-noise ratios are both 30 dB. The number of sampling snapshots is 1024. The parameters of zero-trap width are set to $W_1 = 0.15$ and $W_1 = 0.05$.

The result is shown in Figure 13. As seen in the figure, the beam is formed in several directions and both the sparse interference plus noise covariance matrix reconstruction we mentioned earlier and the asymmetric zero-trap broadening method are applied. Then, we simulated the concentric seven-circle array model. The expected signals come from azimuth 0°, 40°, 40° and pitch 180°, 80°, 300°, and their respective signal-to-noise ratios are 8 dB, 10 dB, and 5 dB. The interference signals come from two directions: azimuth 60°, 240° and pitch 30°, 30°, and their respective signal-to-noise ratios are 30 dB. The number of sampling snapshots is 1024. The final directional diagram is shown in Figure 14. From Figures 14(a) and 14(b), we can see that for the UAV, the concentric circular array model can form the main beam in multiple directions and also uses a sparse INCM to prevent a model mismatch. The zero-trap spreading can also be achieved for interference signals by applying our proposed widening approach for 2D arrays.

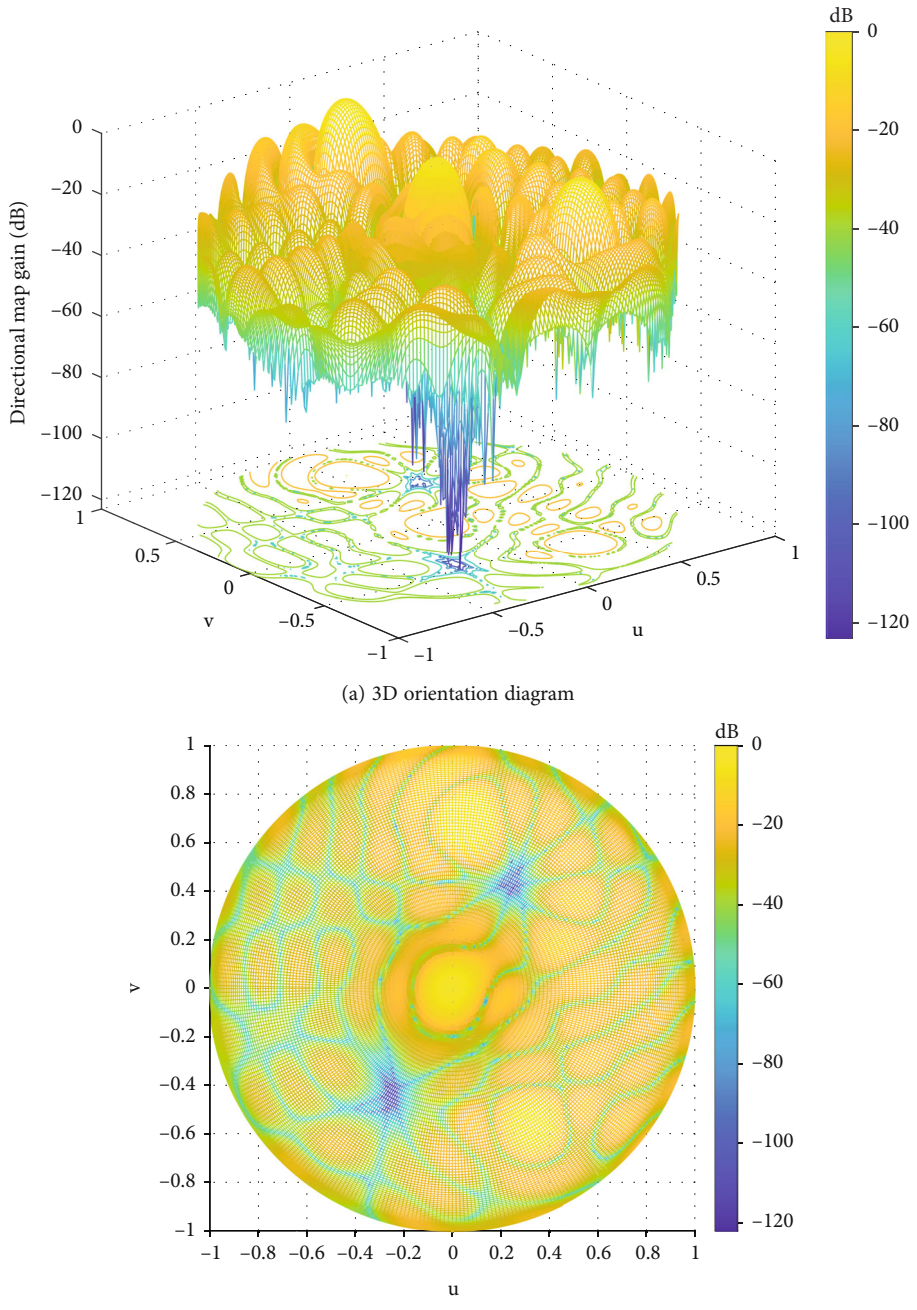

(a) 3D orientation diagram

(b) Top view

Figure 14: Directional map of concentric seven-circle array for multibeam.

Table 2: Comparison of zero-trap widths at different depths for different methods.

	-50 dB	-60 dB	-70 dB	-80 dB	-90 dB	-100 dB
No null widening	0.0455	0.0364	0.0271	0.0187	0.0104	0.0056
CMT [18]	0.0213	0.0115	\	\	\	\
FNW [23]	0.0202	0.0103	\	\	\	\
Proposed methods	0.3273	0.2796	0.2212	0.1905	0.1756	0.1591

5. Conclusion

In this paper, we propose a flexible asymmetric zero trap spreading technique for two-dimensional planar arrays in UAVs to prevent the model mismatch caused by high SNR. We use a sparse covariance matrix reconstruction method in constructing to prevent the model mismatch due to the large SNR of the UAV received signals. And a sparse covariance matrix reconstruction method is used to effectively avoid the model mismatch and to improve the performance of the adaptive beamformer. LCMV is applied to form multiple beams for the case that the UAV may receive multiple signals. Simulation results show that for the UAV planar antenna array, we can reduce the waste of DOF and get a good adjustable zero-notch width. At the same time, the performance of the adaptive beam shaper is still good when the SNR is large. And the main beam can be formed in multiple directions. The results also prove that the proposed method works better in a two-dimensional array and avoids the model mismatch problem compared to some zero-trap spreading approaches. The robustness of UAV antenna adaptive beamforming is enhanced, and the antijamming ability of UAV is improved. In future research, we hope to apply the zero-trap broadening technique to more antenna arrays in different dimensions.

Data Availability

The data used to support the findings of this study are included within the article.

Conflicts of Interest

The authors declare that they have no conflicts of interest.

Acknowledgments

This work is supported by the National Natural Science Foundation of China under Grant Nos. 61901391, 61901382, and 61771404 and the Natural Science Basic Research Plan in Shaanxi Province of China under Grant No. 2020JQ-201.

References

[1] A. Lucieer, D. Turner, D. H. King, and S. A. Robinson, "Using an unmanned aerial vehicle (UAV) to capture micro-topography of Antarctic moss beds," *International Journal of Applied Earth Observation and Geoinformation*, vol. 27, pp. 53–62, 2014.

[2] S. Minaeian, J. Liu, and Y. J. Son, "Vision-based target detection and localization via a team of cooperative UAV and UGVs," *IEEE Transactions on systems, man, and cybernetics: systems*, vol. 46, no. 7, pp. 1005–1016, 2016.

[3] V. V. Klemas, "Coastal and environmental remote sensing from unmanned aerial vehicles: an overview," *Journal of Coastal Research*, vol. 315, no. 5, pp. 1260–1267, 2015.

[4] J. Bendig, M. Willkomm, N. Tilly et al., "Very high resolution crop surface models (CSMs) from UAV-based stereo images for rice growth monitoring in Northeast China," *The International Archives of the Photogrammetry, Remote Sensing and Spatial Information Sciences*, vol. XL-1/W2, pp. 45–50, 2013.

[5] H. L. Van Trees, *Optimum Array Processing: Part IV of Detection, Estimation, and Modulation Theory*, John Wiley & Sons, 2004.

[6] R. Levanda and A. Leshem, "Synthetic aperture radio telescopes," *IEEE Signal Processing Magazine*, vol. 27, no. 1, pp. 14–29, 2010.

[7] Y. Wang, X. Ma, C. Chen, and X. Guan, "Designing dual-tone radio interferometric positioning systems," *IEEE Transactions on Signal Processing*, vol. 63, no. 6, pp. 1351–1365, 2015.

[8] L. Zhao, W. Z. Song, and Y. X. Fast, "Decentralized gradient descent method and applications to in-situ seismic," in *International Conference on Big Data (Big Data)*, pp. 908–917, Santa Clara, CA, USA, 2015.

[9] C. Yang, H. Zhang, F. Qu, and Z. Shi, "Secured measurement fusion scheme against deceptive ECM attack in radar network," *Security and Communication Networks*, vol. 9, no. 16, 3921 pages, 2016.

[10] K. Buckley, "Spatial/spectral filtering with linearly constrained minimum variance beamformers," *IEEE Transactions on Acoustics, Speech, and Signal Processing*, vol. 35, no. 3, pp. 249–266, 1987.

[11] J. Capon, "High-resolution frequency-wavenumber spectrum analysis," *Proceedings of the IEEE*, vol. 57, no. 8, pp. 1408–1418, 1969.

[12] L. L. Horowitz, H. Blatt, W. G. Brodsky, and K. Senne, "Controlling adaptive antenna arrays with the sample matrix inversion algorithm," *IEEE Transactions on Aerospace and Electronic Systems*, vol. AES-15, no. 6, pp. 840–848, 1979.

[13] B. D. Carlson, "Covariance matrix estimation errors and diagonal loading in adaptive arrays," *IEEE Transactions on Aerospace and Electronic Systems*, vol. 24, no. 4, pp. 397–401, 1988.

[14] S. A. Vorobyov, A. B. Gershman, and Z. Q. Luo, "Robust adaptive beamforming using worst-case performance optimization: a solution to the signal mismatch problem," *IEEE Transactions on Signal Processing*, vol. 51, no. 2, pp. 313–324, 2003.

[15] M. Zhang, X. Chen, and A. Zhang, "A simple tridiagonal loading method for robust adaptive beamforming," *Signal Processing*, vol. 157, pp. 103–107, 2019.

[16] A. Hassanien, S. A. Vorobyov, and K. M. Wong, "Robust adaptive beamforming using sequential quadratic programming: an iterative solution to the mismatch problem," *IEEE Signal Processing Letters*, vol. 15, pp. 733–736, 2008.

[17] Y. Gu and A. Leshem, "Robust adaptive beamforming based on interference covariance matrix reconstruction and steering vector estimation," *IEEE Transactions on Signal Processing*, vol. 60, no. 7, pp. 3881–3885, 2012.

[18] Y. Gu, N. A. Goodman, S. Hong, and Y. Li, "Robust adaptive beamforming based on interference covariance matrix sparse reconstruction," *Signal Processing*, vol. 96, pp. 375–381, 2014.

[19] J. R. Guerci, "Theory and application of covariance matrix tapers for robust adaptive beamforming," *IEEE Transactions on Signal Processing*, vol. 47, no. 4, pp. 977–985, 1999.

[20] M. Zatman, "Production of adaptive array troughs by dispersion synthesis," *Electronics Letters*, vol. 31, no. 25, pp. 2141-2142, 1995.

[21] R. J. Mailloux, "Covariance matrix augmentation to produce adaptive array pattern troughs," *Electronics Letters*, vol. 31, no. 10, pp. 771-772, 1995.

[22] Z. Liu, S. Zhao, G. Zhang, and B. Jiao, "Robust adaptive beamforming for sidelobe canceller with null widening," *IEEE Sensors Journal*, vol. 19, no. 23, pp. 11213–11220, 2019.

[23] H. Su, H. Liu, P. Shui, and Z. Bao, "Adaptive beamforming for nonstationary HF interference cancellation in skywave over-the-horizon radar," *IEEE Transactions on Aerospace and Electronic Systems*, vol. 49, no. 1, pp. 312–324, 2013.

[24] Z. Liu, S. Zhao, C. Zhang, and G. Zhang, "Flexible robust adaptive beamforming method with null widening," *IEEE Sensors Journal*, vol. 21, no. 9, pp. 10579–10586, 2021.

[25] Z. Li, J. You, and X. Cai, "Nulling broadening technology based on circular array adaptive beamforming," in *14th international conference on communication technology*, pp. 1123–1128, Chengdu, 2012.

[26] P. S. Naidu, *Sensor Array Signal Processing*, CRC press, 2009.

[27] M. Grant and S. Boyd, *CVX: Matlab software for disciplined convex programming, version 2.1*, 2014.

[28] S. Boyd, S. P. Boyd, and L. Vandenberghe, *Convex Optimization*, Cambridge university press, 2013.

[29] A. Ben-Tal and A. Nemirovski, "Robust convex optimization," *Mathematics of Operations Research*, vol. 23, no. 4, pp. 769–805, 1998.

[30] C. Stearns and A. Stewart, "An investigation of concentric ring antennas with low sidelobes," *IEEE Transactions on Antennas and Propagation*, vol. 13, no. 6, pp. 856–863, 1965.